Structural Characterization of the Antimicrobial Peptide Pleurocidin from Winter Flounder†

Raymond T. Syvitski,‡ Ian Burton,§ Neil R. Mattatall,§ Susan E. Douglas,§ and David L. Jakeman*,‡

College of Pharmacy, 5968 College Street, Dalhousie University, Halifax, Nova Scotia, Canada B3H 3J5, and Institute for Marine Biosciences, National Research Council of Canada, 1411 Oxford Street, Halifax, Nova Scotia, Canada B3H 3Z1

Received March 2, 2005; Revised Manuscript Received March 23, 2005

ABSTRACT: Pleurocidin is an antimicrobial peptide that was isolated from the mucus membranes of winter flounder (*Pseudopleuronectes americanus*) and contributes to the initial stages of defense against bacterial infection. From NMR structural studies with the uniformly ^{15}N-labeled peptide, a structure of pleurocidin was determined to be in a random coil conformation in aqueous solution whereas it assumes an α-helical structure in TFE and in dodecylphosphocholine (DPC) micelles. From ^{15}N relaxation studies, the helix is a rigid structure in the membrane-mimicking environment. Strong NOESY cross-peaks from the pleurocidin to the aliphatic chain on DPC confirm that pleurocidin is contained within the DPC micelle and not associated with the surface of the micelle. From diffusion studies it was determined that each micelle contains at least two pleurocidin molecules.

Antimicrobial peptides (AMPs[1]) serve as a first-line of defense against invading microorganisms. AMPs generally exhibit rapid killing toward a broad spectrum of targets such as Gram-negative and Gram-positive bacteria, enveloped viruses, parasites, and even tumor cells (*1*, *2*). Furthermore, it tends to be difficult for bacteria to develop resistance toward AMPs. Thus, AMPs are being considered as potential alternatives to current antibacterial agents particularly with the emergent problem of drug-resistant pathogenic bacteria (*3*, *4*). AMPs are present in most living organisms, and a wide variety of AMPs have been isolated from many plants and animals (*1*, *5*, *6*); for example, pleurocidin was isolated from the skin mucous secretion of winter flounder (*7*), ceratotoxin was isolated from the female Mediterranean fruit fly (*2*), and shepherin I and II were isolated from the root of the shepherd's purse plant (*8*).

The primary sequences of AMPs can be very different, and range from 12 to 60 amino acids in length (*9*). When folded, the secondary structures consist of α-helices, β-sheets, or both (*9*). Despite the structural variations, AMPs tend to be soluble in both water and membrane environments, are polycationic, and when folded are amphiphilic, having both hydrophobic and hydrophilic domains (*9*). Due to these unique characteristics, AMPs can interact with negatively charged surfaces such as the lipopolysaccharides of Gram-negative bacteria, and can insert into the hydrophobic interior of membranes (*10*). However, beyond this, the underlying mechanism of AMP-mediated cell death is not well understood.

Since L- and D-amino acids (i.e. left- and right-handed α-helixes) function equally well as antimicrobial agents (*11*−*13*), it is generally accepted that AMPs usually associate with the cytoplasmic membrane rather than interact with a specific protein receptor within the membrane (*14*). AMPs can permeate model membrane systems and cause fluorescent dyes and ions to "leak" out of these unilamellar liposomes. For living cells, it is suspected that leakage of essential molecules, which in turn would cause cell death, is due to the formation of ion channels within the cytoplasmic membrane (*15*, *16*). However, for detectable quantities of ion leakage, unnaturally high peptide:lipid ratios (1:10 to 1:50) are typically required (*17*, *18*). Alternatively, AMPs may migrate through the cytoplasmic membrane and inhibit DNA, RNA, and/or protein biosynthesis, ultimately resulting in cell death (*18*, *19*). Regardless, for AMPs to cause cell death they must first associate with and then traverse the cell membrane.

AMPs are continually being secreted from organisms; they are not necessarily expressed as a response to any specific stimulus. When invading bacteria encounter AMPs, the AMPs are suspected to align on, and parallel to the cytoplasmic membrane surface (*20*−*24*). Thereafter, peptides reorient perpendicular to the membrane surface. A number of models have been proposed to describe the specific mode of action including the barrel stave model (*25*), the toroidal pore model (*26*, *27*), and the "carpet-like" model (*28*, *29*). For the barrel-stave model, amphiphilic peptides align perpendicular to the membrane surface and form the staves of a transient barrel of various sizes depending on the number of peptide subunits or staves. The interior of the barrel forms a hydrophilic pore that traverses the cytoplasmic membrane,

† R.T.S. is a recipient of an Izaak Walton Killam Memorial Post-Doctoral Fellowship from the Dalhousie University Killam Trust Foundation.

* Corresponding author. Tel: 902-494-7159. Fax: 902-494-1396. E-mail: David.Jakeman@dal.ca.

‡ Dalhousie University.

§ National Research Council of Canada.

[1] Abbreviations: AMP, antimicrobial peptide; DPC, dodecylphosphocholine; TFE, trifluoroethanol; NOE, nuclear Overhauser effect; NOESY, nuclear Overhauser enhanced spectroscopy; TOCSY, total correlation spectroscopy; HSQC, heteronuclear single-quantum coherence; DOSY, diffusion ordered spectroscopy.

10.1021/bi0504005 CCC: $30.25
Published on Web 04/21/2005

allowing leakage of cytoplasmic contents and causing cell death. The second model is similar, except transient toroidal channels composed of lipids inserted between helical peptides are formed. Again, cell death eventually results from leakage of cytoplasmic contents. For the third model, loss of cell membrane integrity occurs when the membrane becomes covered by a "carpet" of peptides oriented parallel to the membrane surface. Transitory pores are formed, the membrane collapses inward, and the permeability barrier is destroyed. For all three models antimicrobial activity would, in some manner, be accompanied by loss of the pH, salt and/or electrical gradient across the membrane. Consequently, once the peptide traverses the membrane it could continue to migrate into the organism and disrupt DNA/RNA biosynthesis, resulting in cell death.

Pleurocidin is a cationic, 25 amino acid AMP that was isolated from the skin mucous secretion of winter flounder (*Pseudopleuronectes americanus*) and has strong antibacterial activity against Gram-positive and Gram-negative bacteria (*7*). The primary sequence of pleurocidin is 68% and 50% identical to the amphiphilic α-helical dermaseptin from frog skin (*30*) and ceratotoxin from fruit flies (*2*), and both dermaseptin and ceratotoxin are amphiphilic α-helixes. Pleurocidin is predicted to form an amphiphilic α-helix. Analysis of circular dichroism (CD) spectra of pleurocidin dissolved in both TFE and dodecylphosphatidylcholine (DOPC)/dodecylphosphatidylethanolamine (DOPE) vesicles (*31*) confirmed that pleurocidin does form a structure containing between 12% and 24% α-helical content.

From a recent study using macroscopic conductance measurements (*32*), pleurocidin was reported to be only weakly incorporated into neutral bilayers composed of a 7:3 mixture of DOPC and DOPE. However, it was strongly associated with a slightly anionic bilayer of 7:3:1 DOPC, DOPE, and dodecylphosphatidylserine (DOPS) and formed well-defined single ion channels. Similar observations were reported from previous tryptophan fluorescence shift studies (*31*) with the α-helical dermaseptin and ceratotoxin AMPs. Thus, the presence of anionic lipids was concluded to be important for favoring the interaction between lipids and AMPs and, not surprisingly, rationalizes the strong interaction generally observed between these cationic peptides and the anionic outer membrane of Gram-negative bacteria.

Conductance measurements are performed by applying a voltage across the membrane and measuring the current as a function of applied voltage. On the basis of such conductance studies (*32*), it was suggested that pleurocidin may have a resting state where the peptide is lying on the surface of the membrane, and an active state that is induced upon application of the voltage. The peptide is drawn into the membrane and becomes "activated" by the applied voltage. Further to this, it was concluded that pleurocidin either forms toroidal pores or causes the membrane to become permeable by the "carpet" mechanism via the formation of toroidal pores.

Since there is much ambiguity concerning the mode of action of pleurocidin, it is of interest to clarify the molecular structure and interactions of pleurocidin within a membrane-like environment. High-resolution structural data for pleurocidin and pleurocidin-based peptides are crucial for the understanding of the molecular mechanism, as well as improving therapeutic interventions based on these compounds. Pleurocidin is a 2.7 kDa peptide with the amino acid sequence of GWGSFFKKAAHVGKHVGKAALTHYL. From NMR studies of uniformly ^{15}N-labeled pleurocidin in buffered water, in trifluoroethanol (TFE)/buffered water solutions, and in the membrane-like environment of dodecylphosphocholine (DPC) micelles, residue-specific structural and dynamic parameters are determined, and implications for the mode of action are discussed.

Table 1: α-Helical Content of Pleurocidin as a Function of TFE

TFE	0%	5%	10%	15%	20%	25%	30%	35%	40%	45%
% helical content	random	3	5	9	15	22	27	33	35	36

MATERIALS AND METHODS

Peptide Preparation. Synthetic pleurocidin was produced using a solid-phase technique by the Nucleic Acid Protein Service unit at the University of British Columbia. Recombinant pleurocidin was produced in *Escherichia coli* by expressing a codon-optimized gene that fused pleurocidin to an insoluble carrier peptide. The carrier peptide was used to minimize pleurocidin antimicrobial activity during expression and was removed by chemical cleavage, allowing recombinant pleurocidin to be purified by reverse phase chromatography. Uniformly ^{15}N-labeled recombinant pleurocidin was produced by growing and inducing *E. coli*, that expresses pleurocidin, in 500 mL of M9 minimal media using a 2.8 L Fernbach flask. M9 minimal media consisted of M9 salts supplemented with BME vitamin solution (5 mL of 100x stock, Sigma-Aldrich, St Louis, MO) using $(^{15}NH_4)_2SO_4$ (0.6 g) and glucose (2 g) as the sole nitrogen and carbon sources. The cells were grown at 37 °C, 250 rpm, to a cell density of $OD_{595} = 0.8$ and induced. The cells were incubated for an additional 6 h, at which time they were collected by centrifugation. Peptide purity (>95%) and molecular weight for synthetic and recombinant forms of pleurocidin were determined from analysis of HPLC and MS data.

CD Spectroscopy. CD measurements were performed and analyzed to confirm the effects of increasing TFE concentration on the secondary structure of pleurocidin. A stock solution was prepared by dissolving synthetic pleurocidin in 50 mM potassium phosphate-buffered water at pH 6.8. Aliquots of the stock solution were diluted with buffered water and/or TFE to a peptide concentration of 10 μM.

CD spectra for the various solutions were recorded at 298 K on a Jasco J-920 CD spectrometer with a 1 mm quartz cuvette. Spectra were collected and averaged over 16 scans from wavelengths 190 to 250 nm with a 0.1 nm step resolution (Figure 1S, Supporting Information). Analysis of spectra (Table 1) was performed using the CD analysis software DICHROWEB (www.cryst.bbk.ac.uk/cdweb/html/home.html).

NMR Spectroscopy. Samples were prepared by dissolving synthetic pleurocidin in either buffered water (pH of 7.0) or 30% d_2-TFE/buffered water solution to a peptide concentration of 2.0 mM. Samples containing ^{15}N-labeled peptide were prepared by dissolving lyophilized labeled pleurocidin to a concentration of ≈2 mM in 500 μL of buffered water (pH of 7.0). For reconstitution of the ^{15}N-labeled pleurocidin into DPC micelle solutions, an aqueous solution of 1 M DPC (Avanti Polar Lipids, Alabaster, AL) was added to lyophi-

lized pleurocidin to reach the desired peptide:DPC molar ratios (1:1.2, 1:5, and 1:70). After being warmed to 323 K and thoroughly mixed, solutions were lyophilized and rehydrated to a final peptide concentration of ≈2.0 mM with buffered water (pH of 7.0). Thus, the lowest concentration of DPC was 2.4 mM, which is above the DPC critical micelle concentration of 1 mM (*33*). All NMR samples contained 50 mM potassium hydrogen phosphate as the pH buffer and 5% D_2O for the NMR deuterium lock.

As winter flounder seasonally migrates from fresh water to salt water, the salt content of the two pleurocidin samples containing 0 and 140 mM DPC was varied between 0 and 450 mM by adding aliquots of 5 M NaCl. Furthermore, the pH of these solutions was varied between 3.5 and 9.0 using either 5 M HCl or 5 M KOH and measured with a standardized calomel combination pH electrode designed for use with NMR tubes (Aldrich Z11344-1).

^1H and ^{15}N NMR data sets were collected on a Bruker AVANCE 500 spectrometer operating at 500.13 and 50.68 MHz with a triple-resonance, triple-axis gradient probe. ^1H chemical shifts were referenced to 2,2-dimethyl-2-silapentane-5-sulfonate through the water resonance calibrated at each temperature (*34*). ^{15}N chemical shifts were indirectly referenced from the ^1H spectrum (*35*). Unless otherwise stated, ^1H detected spectra were acquired at a repetition rate of 1.5 s^{-1} over the temperature range of 278−313 K with the water frequency centered on the carrier frequency. ^{15}N-decoupled ^1H spectra were acquired with GARP decoupling (*36*) during acquisition over a bandwidth of ≈200 ppm (10 kHz) centered at 110 ppm in the ^{15}N spectrum. Using a standard Bruker pulse sequence, ^{15}N 90° pulse widths were indirectly determined from the ^1H spectra.

One-dimensional (1D) ^1H reference spectra were acquired using a standard one-pulse sequence with presaturation or a "soft" 3−9−19 pulse sequence (*37*, *38*) for suppression of the water signal. NMR data sets were processed using Bruker XwinNMR 3.5. Prior to Fourier transforming, 1D FIDs were apodized using an exponential function with a line broadening of 2 Hz, and zero-filled to twice the number of complex points. 1D "$^{15}N-^1H$ filtered" ^1H data sets were acquired by inserting, immediately before a 3−9−19 pulse sequence, a $^1H-^{15}N$ heteronuclear single quantum correlation (HSQC) pulse sequence (*39*) (with the t_1 increment fixed at 10 μs) as a filter that selects for the resonances of ^1Hs directly bound to ^{15}N centers.

For structural determination, phase-sensitive (*40*), 2D $^1H-^1H$ NOESY (*41*) data sets (see text and figures for mixing times) and $^1H-^1H$ TOCSY (*42*) data sets (MLEV17 (*43*); see text and figures for mixing times) were recorded at 293 K with either a presaturation or a 3−9−19 pulse sequence for water suppression. 2D "$^{15}N-^1H$ filtered" data sets were acquired by inserting a HSQC sequence prior to acquisition. Data sets were collected with 4096 × 512 complex points, apodized with a 70° shifted sine-squared-bell window function in both dimensions, and zero-filled so as to give a final 2D spectrum of 4096 × 2048 real points. Phase-sensitive 3D-$\{^1H-^{15}N\}-^1H$ HSQC-NOESY (*44*) (40 ms mixing time) and 3D $\{^1H-^{15}N\}-^1H$ HSQC-TOCSY (*45*, *46*) (MLEV17; 20 and 60 ms mixing times) data sets were acquired at 293 K with 2048 × 64 × 192 complex points. Data sets were linear predicted (*47*) in both indirect dimensions, apodized using an 80°, 80°, and 90° shifted sine-squared-bell function and zero-filled to give a final 3D spectrum of 2048 × 128 × 512 real points.

Phase-sensitive, 2D $^1H-^{15}N$ HSQC data sets were acquired with a 3−9−19 pulse for water suppression. The ^{15}N dimension contained 128 complex points that covered a sweep width of 26 ppm centered at 119 ppm; in the acquired ^1H dimension, 2048 complex points were collected. Data sets were apodized with a 70° (^1H) and 75° (^{15}N) shifted sine-squared-bell window function and zero-filled so as to produce 2D spectra of 2048 × 512 real points.

In order to assess the dynamics and flexibility of nitrogens along the peptide backbone, ^{15}N relaxation rates and $^{15}N-\{^1H\}$ NOE values were determined from ^1H detected HSQC type data sets (*48*, *49*). For determining ^{15}N spin−lattice (R_1) relaxation rates, 7 linear increments ranging from 13 to 1500 ms were used, and for ^{15}N spin−spin (R_2) relaxation rates, 5 linear increments between 8 and 200 ms were used. ^{15}N R_1 and R_2 values were calculated by fitting the natural logarithm of the peak volume to a linearized single-exponential function using a linear least squares regression program. For $^{15}N-\{^1H\}$ NOE experiments (recovery delay of 7.5 s), two HSQC data sets were acquired with and without ^1H saturation in an interleaved fashion to minimize artifacts. Saturation was achieved by a train of 120° pulses at 5 ms intervals for 4.5 s. $^{15}N-\{^1H\}$ NOE values are reported as peak volume ratios (i.e. V_{ss}/V_0) obtained with (V_{ss}) and without (V_0) ^1H saturation.

To assess the exchange rates of amide protons, samples were lyophilized, rehydrated with 25 μL of H_2O, cooled to 273 K, and then diluted with 475 μL of cold (277 K) D_2O to obtain the 500 μL volume of the original solution. Approximately 5 min after dilution, a series of HSQC data sets (total acquisition time for each HSQC of 5 min) were recorded over a 4 h period at 293 K. The exchange rates of amide protons were further characterized by using equilibrated samples in H_2O and acquiring a series of HSQC data sets at 293 K with and without irradiation of the H_2O signal. Essentially, steady-state nuclear Overhauser effect (NOE) HSQC data sets were recorded by application of a low-powered presaturation pulse to the H_2O signal prior to the HSQC pulse sequence; the H_2O signal was saturated to approximately 80% of its original intensity (determined from a detuned probe). Off-resonance data sets were recorded to provide the reference. To suppress artifacts, recording of on- and off-resonance data was interleaved. The computer difference spectra from the on-resonance, and the off-resonance HSQC spectra generated the fractional intensity change. It is important to note that this method not only can help identify exchanging protons but can detect water molecules in proximity to amide protons by NOE transfer.

Diffusion Ordered Spectroscopy (DOSY) Measurements. DOSY is an accurate and precise method for determining the self-diffusion constant D of a molecular species in solution (*50*, *51*). Since pleurocidin, in its active state, is suspected to associate with membranes, diffusion measurements were performed in order to determine the degree of association between pleurocidin and DPC micelles. Solutions containing ^{15}N-labeled pleurocidin were lyophilized, redissolved in an equivalent volume of D_2O (99.9 atom %D), and transferred into a 5 mm OD, D_2O magnetic susceptibility-matched NMR tube (BMS-3; Shigemi, Tokyo). The

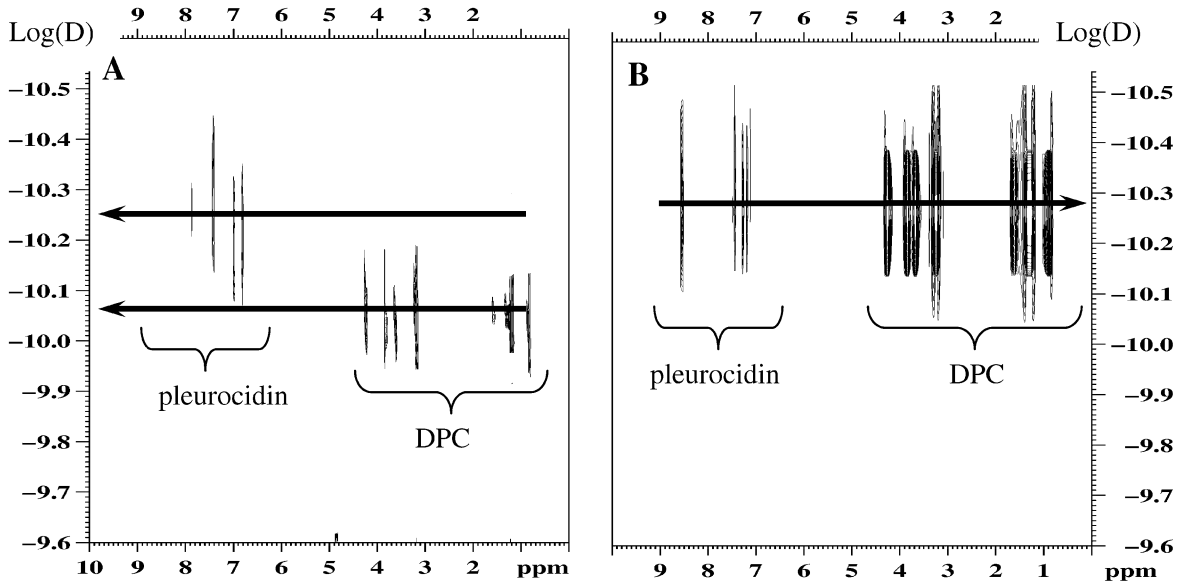

FIGURE 1: From DOSY spectrum of pleurocidin in 140 mM DPC (B), the pleurocidin diffuses with the DPC micelle. However, in 10 mM DPC (A), pleurocidin diffuses as a large (≈50 kDa) aggregate and the DPC diffuses as a smaller micelle independent of the pleurocidin. The F2 dimension of an NMR DOSY spectrum represents the ^{1}H spectrum. The F1 dimension represents log(D) (where D is the self-diffusion constant). DOSY values corresponding to the upfield peaks of pleurocidin are not well resolved in the DOSY dimension for the sample with 10 mM DPC due to overlap with the DPC resonances.

sample height of 1.2 cm ensured that the entire sample was within the radio frequency coils, which is essential for artifact-free and accurate diffusion measurements. ^{1}H detected 2D DOSY data sets were recorded using a stimulated-echo sequence with bipolar-gradient pulses and 32 t_1 blocks of 64 transients each. Careful monitoring of temperature is necessary for obtaining accurate diffusion constants, and thus, the airflow rate, heater power, and inlet air temperature were carefully optimized to achieve a temperature of 293 ± 0.1 K. A recovery delay of 5 ms after each gradient pulse ensured complete dissipation of magnetic eddy currents. The pseudo-2D data sets were processed using Bruker XWinNMR software and consisted of an exponential-multiplication apodization function (lb = 2 Hz) in the F2 dimension prior to Fourier transformation; after F2 linear baseline correction, the t_1 diffusion dimension was processed by fitting the intensity of the resultant F2 peaks to eq 1,

$$I = I_0 \exp(-Dg^2\gamma^2\delta^2(\Delta - \delta/3 - \tau/2)) \qquad (1)$$

where I is the observed intensity, I_0 is the reference intensity (from the unattenuated signal), D is the diffusion coefficient in m^2 s^{-1}, γ is the ^{1}H gyromagnetic ratio (4257.7002 Hz·G^{-1}), δ is the total length of the bipolar defocusing/refocusing gradient pulses, Δ is the diffusion time (0.35 s), and $\tau/2$ is the delay time between the two bipolar gradient pulses which depends on spectrometer constraints. g is the gradient strength that consisted of 32 linear increments between 2.0 and 39.3 G cm^{-1} (5−95% gradient strength) which accounts for the 32 t_1 increments. The duration of the pulsed field gradient δ was optimized (ranged between 0.002 and 0.0035 s) for each sample in order to obtain 5% residual signal with the maximum gradient strength. The error from the fit, 6.10 × 10^{-12} m^2 s^{-1} averaged from all experiments, was determined from the apparent line width in the diffusion dimension. Gradient strength was calibrated by setting the diffusion coefficient of the residual ^{1}H signal from HOD (with no protein) to 2.09 × 10^{-9} m^2 s^{-1} for 293 K.

From the 2D DOSY spectrum of pleurocidin in D_2O, 2 species were observed with different diffusion coefficients, namely, HDO (log D = −8.7) and one protein species (since all of the protein signals correlate to one diffusion constant; log D = −9.98) (Figure 2S, Supporting Information). Therefore, the NMR-measured diffusion constant for pleurocidin at 293 K was 12.8 × 10^{-11} m^2 s^{-1}. For the DOSY spectrum of pleurocidin in 140 mM DPC two species were present, HDO, and pleurocidin with DPC (log D = −10.31) (Figure 1). The pleurocidin and DPC micelle migrated at the same rate and thus had, to within experimental error, the same diffusion constant of 4.9 × 10^{-11} m^2 s^{-1}. Interestingly, for the sample of pleurocidin in 10 mM DPC there are 3 distinct diffusing species: HDO, DPC (log D = −10.17), and pleurocidin with DPC (log D = −10.31) (Figure 1). The majority of DPC is diffusing at 6.76 × 10^{-11} m^2 s^{-1} and not with the pleurocidin at 4.90 × 10^{-11} m^2 s^{-1}.

ANALYSIS AND RESULTS

NMR Spectroscopy. NMR spectra were analyzed, and peak positions and peak volumes were determined using Sparky 3.110 software (*52*) operating on a Linux PC system. For structural determination, all spin systems of pleurocidin in buffered water (pH 6.8, 0 mM NaCl), TFE/buffered water (30% TFE, pH 6.8, 0 mM NaCl), and DPC micelles (140 mM DPC, pH 6.8, 0 mM NaCl) were identified through chemical shifts and characteristic TOCSY cross-peak patterns. For pleurocidin in buffered water and TFE/water, no ^{15}N−^{1}H filtering was required and thus cross-peaks to non-H^N resonances could be observed (Figures 3S and 4S, Supporting Information). However for pleurocidin in DPC, ^{15}N−^{1}H filtering was required and only connections to H^N resonances could be observed (Figure 5S, Supporting Information). For all samples, the resonance of the Trp2 aromatic

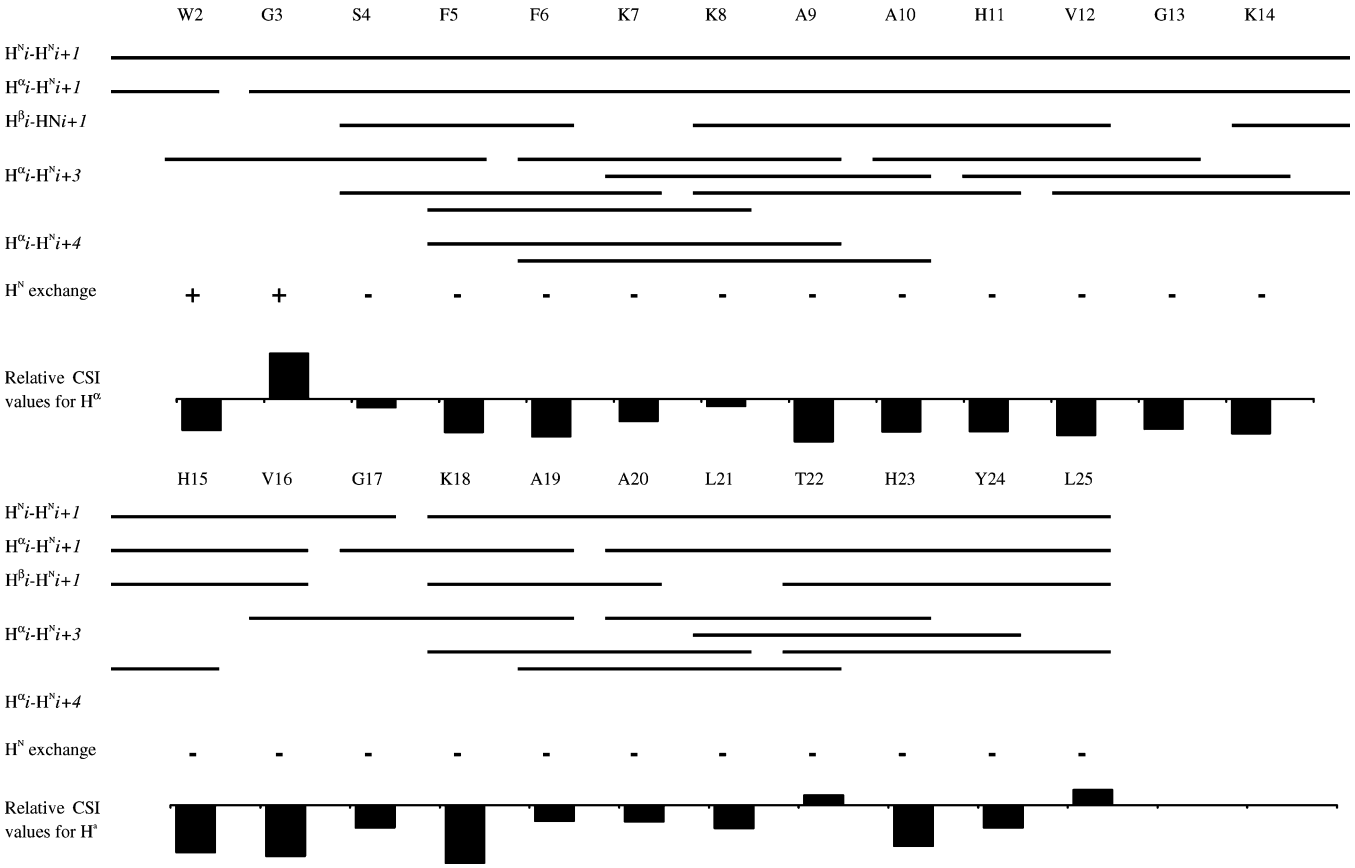

FIGURE 2: From the sequential and longer range NOESY connections, H^N exchange properties, and H^α CSI values for pleurocidin in 140 mM DPC, structural constraints were determined and used with the simulated annealing program XPLOR.

side chain and residues Ser4 and Thr22 were readily assigned from their unique TOCSY patterns, since each residue occurs only once in the sequence. Starting from these assigned residues, sequence-specific assignments of backbone and side chain resonances (except for Gly1 in buffered water and Gly1, Gly3-Phe5, Tyr24, and Leu25 in 30% TFE; Table 1S, Supporting Information) were determined (*53*).

For pleurocidin in buffered water, only interresidue NOESY cross-peaks from residues *i* to $i + 1$ were observed (Figure 6S, Supporting Information). However for pleurocidin in TFE/water, besides the short range (*i* to $i + 1$) interresidue connections, cross-peaks between residues *i* and $i + 3$ were observed for residues between Phe6 and Val12 (Figure 7S, Supporting Information). For pleurocidin in 140 mM DPC, besides short-range connections, cross-peaks between *i* and $i + 3$ (and some *i* and $i + 4$) were observed for residues Trp2 to Leu25 (Figures 8S (Supporting Information) and 2). Since this sample required $^{15}N-^{1}H$ filtering, no $H^{\alpha}_{i}-H^{\beta}_{i+4}$ connections could be observed. Nevertheless, more than 215 unique cross-peaks were assigned from the 120 ms NOESY spectrum and 171 from the 3D HSQC-NOESY (Figure 9S, Supporting Information). Due to the slow reorientational motion of pleurocidin in DPC micelles, NOESY cross-peaks could result from efficient spin-diffusion. However, by comparing NOESY spectra at various mixing times, very few cross-peaks were identified as arising from spin-diffusion.

An important factor when determining peptide structure is the presence of hydrogen bonds that stabilize secondary and tertiary structures. Hydrogen bonds were partially assessed by amide hydrogen exchange rates (*54*). Since at high concentrations pleurocidin disrupts membrane structure, rehydrating a lyophilized pleurocidin/DPC sample most likely caused a redistribution of the DPC micelle structure exposing the H^N protons of pleurocidin to the D_2O solvent. Thus H^N protons exchanged more rapidly than could be monitored with NMR spectroscopy (i.e. within 5 min). Thus, steady-state NOE experiments on equilibrated samples were used to observe either directly exchanging protons or transfer of magnetization from H_2O to H^N protons (Figure 3). For pleurocidin in 0 and 2.4 mM DPC, significant magnetization transfer after 50 ms of water peak irradiation was observed due to direct proton exchange. Significant magnetization transfer due to NOE relaxation pathways is not likely to occur at such short mixing times for a relatively fast tumbling peptide and H_2O molecules. Thus, at 0 and 2.4 mM DPC the amide protons on pleurocidin are "unprotected" and are not involved in hydrogen bonding or surrounded by a hydrophobic envelope from DPC molecules. For pleurocidin in 140 mM DPC, no significant magnetization transfer was observed for residues Ser4−Leu25 even after 500 ms of water irradiation (Figure 3). Water is neither readily exchanging nor in the vicinity of the backbone H^N protons of residues Ser4−Leu25. Furthermore, amide exchange rates are affected by pH. At high pH in 0 and 2.4 mM DPC H^N protons were not readily observable in 1D spectra due to the rapid exchange of H^N with H_2O. However, even at high pH for pleurocidin in 140 mM DPC the intensity of 1D peaks for residues Ser4−Leu25 did not significantly decrease; residues near the N- or C-terminus have a more pronounced pH effect but not to the same extent as pleurocidin in 0 or 2.4 mM DPC (Figures 10S and 11S, Supporting Information).

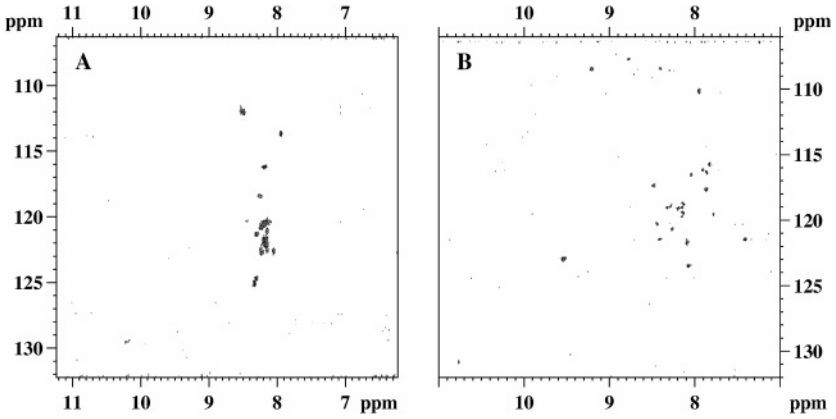

FIGURE 3: The H^N exchange properties were identified from steady-state HSQC difference spectra of pleurocidin in buffered water (A) and 140 mM DPC (B). For spectrum A, the water signal was irradiated for 50 ms whereas for spectrum B it was irradiated for 500 ms. As observed by the weak signals in spectrum B, even after 500 ms, H^N protons of pleurocidin in 140 mM DPC do not readily exchange.

Since H^N and H^α resonances are sensitive to the proton environment, preliminary information on protein or peptide secondary structure can be derived by comparing the H^α chemical shifts to random-coil values (*55*, *56*). From the chemical shift index (CSI) values, the H^α resonances of amino acids that are part of an α-helical structure tend to shift upfield, whereas resonances for *β*-sheet structures tend to shift downfield compared to random-coil chemical shifts. For pleurocidin in buffered water, ^1H resonances are clustered into well-defined narrow regions. For example, resonances from aromatic protons are within the region between 7.0 and 7.4 ppm, H^N resonances fall within the region between 8.0 and 8.8 ppm (Figure 4) and H^α resonances are within the region between 4.1 and 4.7 ppm. As the concentration of DPC was increased beyond 2.4 mM DPC, the chemical shifts of resonances corresponding to aromatic, H^N and H^α protons dispersed; for example, resonances from aromatic protons are distributed within the region between 7.0 and 7.7 ppm for 10 mM DPC, and 6.9 and 7.8 ppm for 140 mM DPC, H^N resonances fall within the region between 7.4 and 8.8 ppm for 10 mM DPC and 7.4 and 9.4 ppm for 140 mM DPC, and H^α resonances are distributed within the region between 3.8 and 4.7 for 140 mM DPC. Most H^α resonances shifted upfield (Table 1S) with increasing DPC concentration which is indicative of α-helical formation.

Structure Calculations. For structure calculations, distance restraints determined from integration of NOESY cross-peaks (from 400 ms NOESY spectra for pleurocidin in H_2O and TFE, and the 120 ms and 40 ms NOESY for pleurocidin in 140 mM DPC) were classified into four groups: strong, medium, weak, and very weak corresponding to interproton distances ranges of <2.3, 2.0−3.5, 3.3−5.0, and 4.8−6.0 Å (Table 2S, Supporting Information). Assessment of hydrogen bonding was carried out on the basis of the presence of H^α_i−H^N_{i+3} and H^α_i−H^N_{i+4} connectivity in the NOESY spectrum of pleurocidin in 140 mM DPC, the exchange rates for the amide protons, and the CSI values (*55*, *56*). For residues determined to be involved in hydrogen bonding (residues Trp2−Leu25 for pleurocidin in 140 mM DPC and Phe6−Val12 for pleurocidin in TFE), hydrogen bonds between CO_i and H^N_{i+4} were included as constraints by restraining r_{H-O} to 1.2−1.9 Å and r_{N-O} to 1.8−2.9 Å (*57*, *58*). For pleurocidin in 140 mM DPC, a total of 143 inter-residue constraints (103 sequential and 40 intermediate range ($i + 2$ to $i + 4$)) were identified (Table 2S).

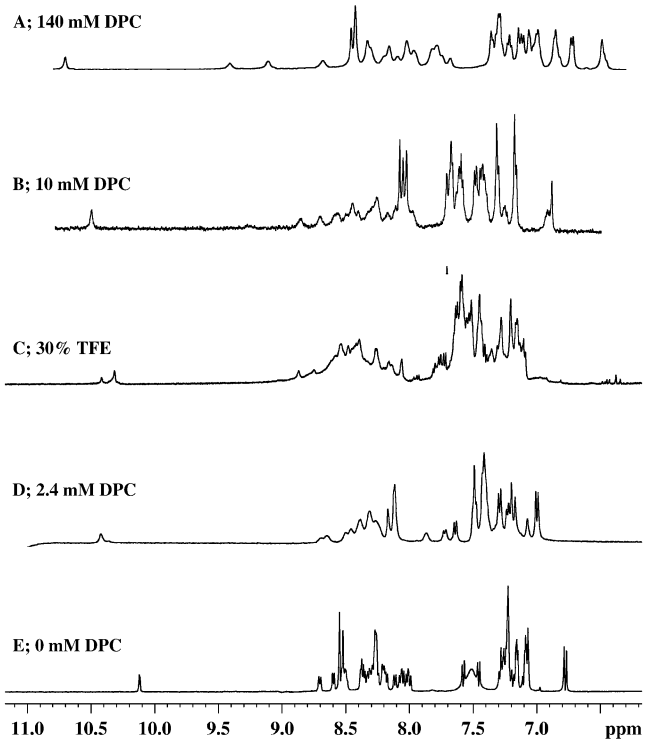

FIGURE 4: From the downfield spectral regions of pleurocidin in DPC and in TFE, the HN and aromatic signals disperse with increasing DPC or TFE concentration, which is indicative of the formation of defined structural elements. The signals of synthesized pleurocidin in 30% TFE/water are broad due to impurities; however, the distribution of resonances is similar to that of pleurocidin in 10 mM DPC.

All structural calculations were based on previous studies (*59*) using the XPLOR 3.1 (*60*−*62*) software package. Briefly, an initial random coil extended structure was used to generate a total of 100 embedded structures. Close contacts were removed by energy minimization of 1000 conjugate gradient steps before proceeding to the restrained simulated annealing molecular dynamics (MD) calculations. Eight steps comprising a total simulation time of 120 ps were used for the MD simulations. Initially, the system was set to 1500 K and all force constants for bonded, NOE, dihedral angle and nonbonded interactions were scaled to 10% of their full values. By the end of the third step, the force constants had been linearly scaled to their full values. In the last five steps

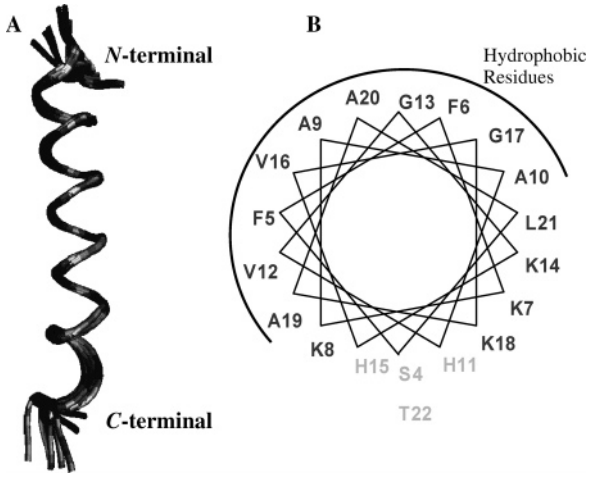

FIGURE 5: Structural constraints determined from NMR data were used with computer simulations to calculate structures for the pleurocidin peptide in DPC micelles; the structures that did not violate any structural constraints were retained (A; not all structures shown). For the α-helical wheel of pleurocidin (B), hydrophobic residues are clustered around approximately 2/3 of the α-helix whereas basic and hydrophilic residues comprise the remaining 1/3.

the temperature was decreased uniformly to 300 K. Calculated structures were then energy minimized with 2000 conjugate gradient steps. A total of 21 lowest-energy structures (Figure 5) were retained that had no violations of NOESY constraints >0.5 Å. The overall quality of these refined structures was examined with the program PROCHECK (*63*−*65*). Except for random-coil sections, all backbone dihedral angles resided in the well-defined, acceptable regions of the Ramachandran plot.

Pleurocidin Structure. In agreement with current and previous results from CD studies, no portion of pleurocidin in buffered water could be identified as having a well-defined structure, as reflected in the CSI values and lack of $H^{\alpha}_{i}-H^{N}_{i+3}$, $H^{\alpha}_{i}-H^{N}_{i+4}$, or $H^{\alpha}_{i}-H^{\beta}_{i+3}$ connections. Furthermore, sequence-specific assignments could only be accomplished through the $H^{\alpha}_{i}-H^{N}_{i+1}$ NOESY connections as most $H^{N}_{i}-H^{N}_{i+1}$ connections were not observed due to rapid proton exchange with water. Analysis of NOE difference HSQC spectra confirmed that H^N protons are exchanging rapidly, as significant magnetization transfer after 50 ms water peak irradiation was observed. Since the chemical shifts of the H^N and ^{15}N resonances of pleurocidin in 2.4 mM DPC are virtually identical to those in 0 mM DPC, and similar proton exchange rates are observed for all amide protons (i.e. amide protons are unprotected), it is likely that pleurocidin in 2.4 mM DPC has no well-defined secondary structure.

At 30% TFE there are midrange NOESY connections between Phe6 and Val12, and not surprisingly from the calculated structure, an α-helical structure exists between these residues. The extent of the calculated α-helical structure is ≈25%, which is in accordance with that estimated from current and previous CD spectral analysis (Table 1). Since the chemical shifts of resonances of pleurocidin in 10 mM are similar to the resonances of pleurocidin in 30% TFE, it is likely that pleurocidin in 10 mM DPC is partially α-helical. However, as the structure has not yet been determined, the location and extent of the α-helix structure cannot yet be identified.

From the overlaid nonviolating structures of pleurocidin in 140 mM DPC, pleurocidin forms an amphiphilic α-helix between residues Trp2 and Leu25 with an rmsd of 0.51 Å for the backbone and 1.2 Å for all heavy atoms in this region. No evidence from the NOESY data or calculated structures would indicate that the helix is distorted or bent. The helix extension is in accordance with amide protons having very slow exchange, the midrange NOESY connectivity, and the CSI values.

Although NOESY data were not acquired at all DPC, pH, salt, and temperature conditions, ^1H chemical shifts are diagnostic of structural elements. For all samples, pH, salt, and temperature variations had minor effects on ^1H chemical shifts of nonexchangeable protons. For exchangeable amide protons, increasing the pH or temperature caused a slight monotonic upfield shift in both H^N and ^{15}N resonances, whereas increasing salt concentration had virtually no effect. The lack of large chemical shift changes is indicative of the lack of structural changes within the peptide upon varying pH, salt concentration, or temperature (Figures 10S and 11S, Supporting Information).

Pleurocidin/DPC Structural Characteristics. An interesting feature observed in the NOESY spectra of pleurocidin in DPC (2.4, 10, and 140 mM) was the presence of strong NOESY cross-peaks between the H^N protons on pleurocidin and the protons of the DPC molecules. Since solutions containing 2.4 and 10 mM DPC did not present a significant dynamic range problem, no $^{15}N-^1H$ filtering was required and thus NOESY cross-peaks between the DPC and side-chain protons could be identified. Various NOESY mixing times were utilized in order to identify non-spin-diffusion NOESY cross-peaks and in turn estimate distances between amino acids on the pleurocidin and DPC protons.

Within the ^1H NMR spectrum of DPC, the protons of the lipophilic terminal $-CH_3$ group are assigned to the resonance at $\delta = 0.97$ ppm, the $-(CH_2)_9-$ groups are overlapping at $\delta = 1.38$ ppm, the $-CH_2-$ group adjacent to the phosphate group is at $\delta = 1.7$ ppm, and the $-N^+(CH_3)_3$ group is at $\delta = 3.35$ ppm, and all other methylene proton resonances are at lower field than 3.5 ppm (Figure 6). For this system, spin-diffusion does not seem to be efficient, as no consistent links between the methyl and methylene protons of the hydrophobic tails of DPC were observed. Thus, connections between the peptide and the terminal methyl group on the DPC molecule are likely a result of direct NOE transfer and not spin-diffusion. Three residues could be identified as having a direct NOE from the H^N to the methyl group, namely, Ala9, Val12, and Lys14, which are near the center of the peptide sequence; although the cross-peak intensities are low, these cross-peaks are observed in duplicate and shorter mixing time NOESY experiments. Furthermore, cross-peaks were only observed for these three residues and, thus, the cross-peaks are likely from direct NOE transfer and not spin-diffusion. Intermolecular NOEs between all amide protons of pleurocidin and the $-(CH_2)_9-$ groups of DPC were observed. The intensities of these intermolecular NOEs are largest for residues located centrally and decrease toward the ends of the peptide. In the NOESY spectra, intermolecular NOEs were identified from the $-N^+(CH_3)_3$ group at $\delta = 3.35$ ppm to the amide backbone protons of Trp2, Gly3, His23, Tyr24, and Leu25, and the Trp2 side chain.

Diffusion NMR. From the determined *D*, the hydrodynamic radius r' and subsequently an estimate of the molecular mass of the diffusing species (*51*, *66*) can be calculated using the

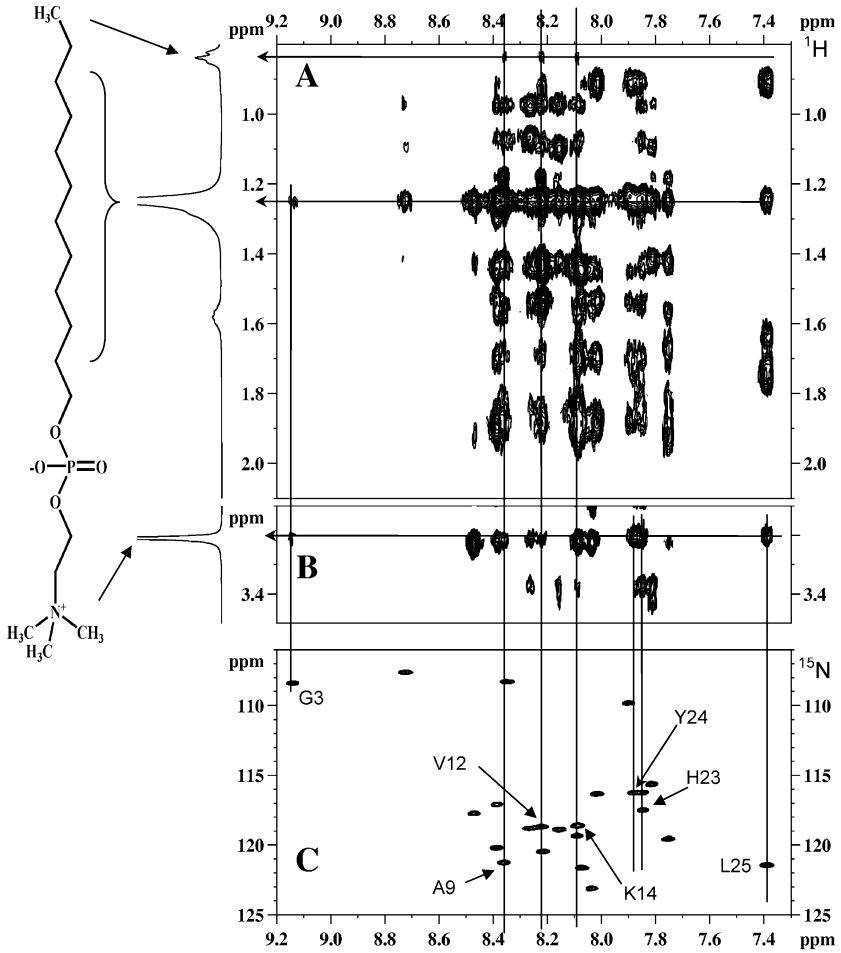

FIGURE 6: From the downfield region of the 500 ms NOESY (A and B) and HSQC (C) spectrum of pleurocidin in 140 mM DPC, NOESY connections are observed from the DPC to pleurocidin. The terminal G3 and W2 side chain (not shown), L25, Y24, and H23 N^H backbone have connections to the choline methyls whereas the entire H^N backbone has correlations to the CH_2s and A9, V12, and K14 have correlations to the terminal CH_3 group on DPC. Connections to A9, V12, and K14 are observed in duplicate NOESY experiments as well as NOESY experiments with shorter mixing times.

Stokes−Einstein equation (eq 2),

$$D = kT/(6\pi\eta r') \quad (2)$$

where k is the Boltzmann constant, T is the absolute temperature, and η is the bulk viscosity of the solution which is a function of solution conditions (e.g. temperature, salt, and protein concentration). The η of each solution was estimated from the diffusion constant of the residual HDO signal (e.g. for pleurocidin in 0 and 140 mM DPC, η was estimated to be 1.4×10^{-3} and 1.5×10^{-3} kg m^{-1} s^{-1}).

From the calculated r' ($\approx 1.1 \times 10^{-9}$ and 2.9×10^{-9} m for pleurocidin in 0 and 140 mM DPC) the molecular mass (MM) in daltons can be estimated (eq 3) by relating the equation of the volume of a sphere to the partial specific volume of a protein V_p. The V_p of an average protein is estimated to be 0.73×10^{-6} m^3 Da^{-1} (*66*, *67*). The protein/micelle assembly is also assumed to have a V_p of approximately 0.73×10^{-6} m^3 Da^{-1}.

$$r' = \{[(4)(0.73 \times 10^{-6})(\mathrm{MM})]/[(3\pi)(6.023 \times 10^{23})]\}^{1/3} \quad (3)$$

On the basis of these calculations the molecular mass of pleurocidin in aqueous solution is calculated to be 3.0 kDa, which is very close to the theoretical mass of 2.7 kDa. The molecular mass of the pleurocidin/DPC micelle is calculated to be ≈50 kDa whereas the molecular mass of DPC micelles that are not associated with pleurocidin is calculated to be ≈20 kDa, close to the expected protein-free molecular mass of DPC micelles (19 kDa) determined form a previous study (*68*).

Backbone Dynamics. Peptide backbone dynamics and flexibility were assessed using the Lipari−Szabo formalism (*69*−*72*) with the Modelfree 4.15 software package (*73*, *74*). The square of the generalized order parameter S^2, the exchange rate constant R_{ex}, the effective correlation time for fast internal motions t_e, and the global reorientational tumbling time t_m were assessed from the experimentally measured R_1, R_2, and NOE values. For pleurocidin in 0 mM DPC, the NOE and calculated S^2 values are low ($0.2 < S^2 < 0.3$), which is consistent with nonrestricted internal motion and a random coil structure. No further analysis of the relaxation data for pleurocidin in 0 mM DPC was performed.

For pleurocidin in 140 mM DPC, relatively high NOE values (>0.6) (Figure 12S, Supporting Information) are indicative of residues that are located in regions with restricted internal motions. The R_2/R_1 ratio for those residues whose relaxation is not affected by the fast internal motions (on the picosecond time scale) was virtually independent of the internal motion and provides an initial estimation for the reorientation time of all N−H vectors with a global tumbling

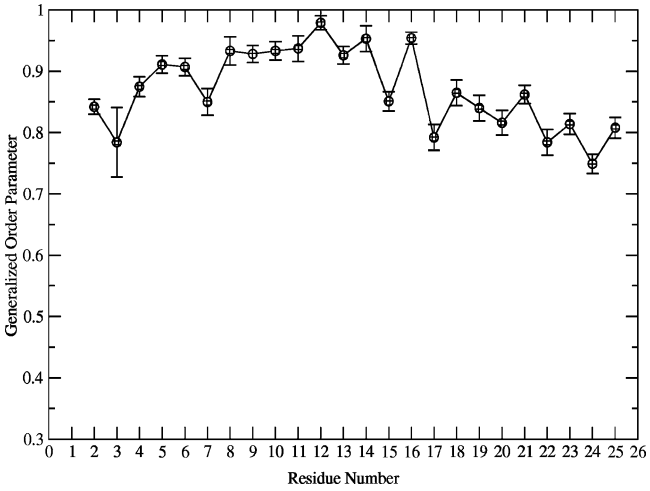

FIGURE 7: From the calculated generalized order parameters S^2 for backbone H^N vectors of pleurocidin in 140 mM DPC, all residues have restricted motion; residues near the N- and C-terminus have slightly more motional freedom. The S^2 parameter is a measure of dynamic behavior of the H^N bond vector and varies between 1 and 0. A value of 0 represents complete motional flexibility whereas a value of 1 represents complete rigidity. Values of S^2 between 0.85 and 1.0 are typical of a well-defined structure.

time t_m. Initial estimates of the t_m value in DPC obtained from the R_2/R_1 ratio and averaged over all residues yielded a value of 11.1 ns.

Using calculated structural data for pleurocidin in 140 mM DPC and ^{15}N relaxation data as input, the parameters of the molecular rotational diffusion tensor were calculated. The appropriate model of dynamics for each given spin was then selected, as outlined in a previous study (*73*, *74*). To assess the fit of any single model to the relaxation data, confidence limits were estimated on the basis of 300 Monte Carlo simulations. It was found that all of the relaxation data were best fitted to the model of dynamics with only one or sometimes two model-free parameters, S^2 and if necessary t_e. The t_e values were on the order of tens to hundreds of picoseconds, and the exchange contribution R_{ex} was insignificant. For the final calculations, the t_m value was optimized simultaneously with appropriate dynamics parameters (S^2 and t_e) for the backbone N−H vectors of each residue. The optimized t_m value for pleurocidin in DPC was 12.0 ns with a diffusion asymmetry of 1.34 and the long axis collinear with the long axis of the pleurocidin α-helix. This value is very close to those estimated from the R_2/R_1 ratio, thus suggesting the absence of significant contributions of exchange and slow internal motions. All amide protons have similar motional characteristics with order parameters S^2 between 0.83 and 0.97 (Figure 7) consistent with well-defined secondary structural elements; amide protons near the N- or C-terminal regions tend to have S^2 slightly less than 0.85, which is indicative of slightly more motional freedom near the terminus.

DISCUSSION

On the basis of NOESY connections, CSI values, analysis of ^{15}N relaxation data, and CD data, the structures of pleurocidin in 0 mM DPC, 30% TFE, and 140 mM DPC were determined. Confirming previous CD studies, pleurocidin in 0 mM DPC has no identifiable well-defined secondary structure. On the basis of the similarity of chemical shifts between samples with 0 and 2.4 mM DPC, it is likely that pleurocidin in 2.4 mM DPC also has no well-defined secondary structure.

As the DPC concentration was increased to 10 mM, the proton chemical shifts dispersed and were similar to the chemical shifts observed for pleurocidin in 30% TFE. Thus it is taken that pleurocidin in these two solutions have similar structures. The structure of pleurocidin in 30% TFE was determined to be α-helical between residues Phe6 and Val12, which accounts for ≈25% of the peptide and is in accordance with current and previous CD studies.

Pleurocidin in 140 mM DPC was calculated to be α-helical between residues Trp2 and Leu25. This represents ≈95% α-helical content. The helical extent is significantly longer than was reported in previous CD studies with pleurocidin in membrane environments (12% in DOPC and 24% in 3:1 DOPC/DOPE mixture) (*31*). This may be due to the inaccuracies associated with CD analysis or reflect the effects of various membrane-like environments on the structure of proteins and peptides (*68*, *75*). Current studies with pleurocidin focus on the effects of different membranelike environments, including DOPC, DOPE, and DOPS mixtures on pleurocidin structure.

The dynamic properties of pleurocidin in 140 mM DPC are in agreement with the presence of a well-defined stable secondary structure. High NOE and S^2 values were obtained for all residues, which is indicative of restricted internal motions of the amide bond vectors. Residues near the N- or C-terminus have slightly lower S^2 values and thus slightly more motional freedom. The t_m value in DPC was found to be 12.0 ns, which is similar to the values typically obtained (8−20 ns) for peptides of comparable size in micelles (*76*, *77*). For the most part, neither the R_{ex} or t_e values were required to reasonably fit the ^{15}N relaxation data. Thus, pleurocidin in DPC micelles is not subject to extensive conformation exchange or internal motions on the nanosecond to picosecond time scale. The absence of these significant complicating effects of the peptide dynamics manifested itself in the similarity of optimized t_m values to those estimated from the R_2/R_1 ratio.

When determining the ^{15}N T_1 and T_2 values, the integrated peak volumes were very well defined by a single-exponential function, which indicates that the motional freedom of the peptide (i.e. both t_m and S^2) was identical for all molecules. Thus, for pleurocidin in 140 mM DPC, all the diffusing species that contain pleurocidin are of uniform size and molecular mass, which from diffusion measurements was estimated to be ≈50 kDa. For a pleurocidin−DPC species to diffuse at ≈50 kDa, this would require, for example, 1 pleurocidin molecule surrounded by ≈150 DPC molecules, or 2 pleurocidins surrounded by ≈140 DPCs, etc. As the molar ratio of pleurocidin:DPC is only 1:70, the diffusing species must contain at least two pleurocidin molecules (and, thus, ≈140 DPC molecules), which is in accordance with other membrane-associated proteins (*78*). The possibility of dimerization and, thus, the structure of the pleurocidin−DPC micelle cannot be assessed with the current isotopic labeling scheme. Further studies with $^{15}N/^{13}C$-labeled pleurocidin at a variety of peptide:DPC ratios are underway to address the possibility of pleurocidin aggregation.

The findings presented here can be compared with results from studies of other membrane proteins in micelles. From

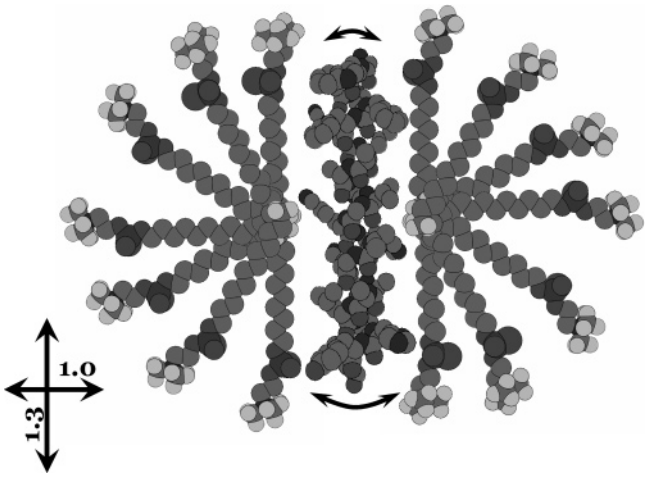

FIGURE 8: On the basis of NOESY connections, DPC molecules align approximately parallel to the α-helical axis of pleurocidin. From ^{15}N relaxation data, the assembly has a structural asymmetry of about 1.3. From the S^2 values, the N- and C-termini have slightly more motional freedom than the central portion of the peptide. From DOSY experiments it was determined that there are on average 2 pleurocidin and 140 DPC molecules for each micelle. As the relative positions of the 2 pleurocidin molecules cannot be determined from these experiments, this diagram is a schematic representation. The number and position of the peptides within a micelle is part of an ongoing investigation.

previous studies of a bacteriophage coat protein in SDS micelles, the presence of two membrane-associated helices with different motional characteristics had been demonstrated (*76*, *77*), namely, a transmembrane helix with an average S^2 of ≈0.88 and a surface associated helix with an average S^2 of ≈0.65. Values of R_2, NOE, and S^2 for pleurocidin were almost identical to those values determined for the transmembrane helix of the bacteriophage coat protein.

Additional to this, there are NOESY connections throughout the pleurocidin backbone to the aliphatic $-CH_2-$ groups on DPC. Connections to the terminal methyl on the aliphatic side chain of DPC are only observed to residues Ala9, Val12, and Lys14, which are in the middle of the pleurocidin structure. The methyls of the choline group have NOESY connections to the N- and C-terminal residues only. Therefore, the DPC molecules that are in contact with the helix align approximately parallel to the pleurocidin α-helical axis allowing the N- and C-terminal residues to contact the choline methyls; the amide protons along the backbone contact the aliphatic $-CH_2-$ groups, and the residues near the middle of the α-helix contact the terminal aliphatic methyl group (Figure 8). The N- and C-terminal groups most likely form electrostatic interactions with the positively charged choline group. For example, the C-terminal carboxyl group and the indole proton of the Trp2 residue can form a strong electrostatic interaction (which may also include hydrogen-bonding interactions) with the positively charged choline group (*79*, *80*).

The NOEs between pleurocidin and the DPC molecules are all negative in sign. Thus, the "lifetime" of an individual DPC molecule which is in contact with the peptide is longer than ≈0.3 ns (*81*). However, from the observation that there are a single set of DPC chemical shifts, the lateral mobility of individual DPC molecules is on the sub-millisecond time scale.

From ^{15}N relaxation data and the observed DPC−pleurocidin NOEs, it is unlikely that pleurocidin resides on the surface of the neutral micelle; DPC forms a hydrophobic phase that surrounds the peptide (Figure 8). However, from DOSY analysis, there are 2 pleurocidins for each micelle. It is possible that the hydrophobic sides of the peptide associated, but this cannot be assessed with the current isotopic labeling scheme.

An interesting feature of pleurocidin in 10 mM DPC (pepide:lipid ratio of 1:5) is the absence of a well-defined structure (Figure 4), but the presence of strong NOESY cross-peaks from pleurocidin side chain protons to the aliphatic $-CH_2-$ groups of the DPC molecules. In addition, pleurocidin diffuses as a very large (≈50 kDa) species. However, the majority of the DPC molecules diffuse as a species of about 20 kDa. As most of the 10 mM DPC is not associated with the ≈50 kDa pleurocidin species, the pleurocidin itself must be aggregating (e.g. ≈20−25 pleurocidin molecules per species). Investigations are ongoing, as this might be an indication that high concentrations of pleurocidin form pores within a membrane environment or disrupt the membrane environment by aggregation.

Considering that membrane proteins need to be extracted from their natural environment and reconstituted in artificial micelles for 3D structure determination, comparative studies of the protein interactions with the different environments are of special interest. The present results have led to the stoichiometry of pleurocidin/DPC micelles in aqueous solution, and a structural characterization of the interaction between the two components of the mixed micelles.

This work provides a first investigation of the structure and backbone dynamics of pleurocidin in a membrane-like environment. Our findings provide the necessary scaffold for subsequent studies on pleurocidin interactions with other membrane environments and for addressing the dynamics of antimicrobial peptide pore formation within membranes.

ACKNOWLEDGMENT

John Walter has provided thoughtful discussions. We thank Alison Thompson for the use of the CD instrument and Brian Bryksa for purifying the ^{15}N-labeled pleurocidin. This is NRC publication number 2005-42491.

SUPPORTING INFORMATION AVAILABLE

Twelve figures and 2 tables, including figures of the CD trace for pleurocidin in various concentrations of TFE, 120 ms TOCSY and 400 ms NOESY of pleurocidin in buffered H_2O, 90 ms TOCSY and 400 ms NOESY of pleurocidin in 30% TFE/H_2O, 60 ms ^{15}N-filtered TOCSY and 120 ms NOESY of pleurocidin in 140 mM DPC, schematic representation of the number of NOESY constraints per residue, 1D spectra of pleurocidin in buffered H_2O and 140 mM DPC at various pHs, DOSY spectra of pleurocidin in 0 and 2.4 mM DPC, and experimental and fitted ^{15}N relaxation values and tables of chemical shifts and structural constraints. This information is available free of charge via the Internet at http://pubs.acs.org. The structural coordinates (1Z64) have been deposited in the Protein Data Bank (http://www.pdb.org/).

REFERENCES

1. Hancock, R. E. W., and Lehrer, R. (1998) Cationic peptides: a new source of antibiotics, *Trends Biotechnol. 16*, 82.

2. Marri, L., Dallai, R., and Marchini, D. (1996) The novel antibacterial peptide ceratotoxin A alters permeability of the inner and outer membrane of *Escherichia coli* K-12, *Curr. Microbiol. 33*, 40.
3. Hancock, R. E. W. (1999) Host defence (cationic) peptides—What is their future clinical potential?, *Drugs 57*, 469.
4. Hancock, R. E. W. (2000) Cationic antimicrobial peptides: towards clinical applications, *Expert Opin. Invest. Drugs 9*, 1723.
5. Boman, H. G. (1996) Peptide antibiotics: Holy or heretic grails of innate immunity?, *Scand. J. Immunol. 43*, 475.
6. Ganz, T., and Lehrer, R. I. (1998) Antimicrobial peptides of vertebrates, *Curr. Opin. Immunol. 10*, 41.
7. Cole, A. M., Weis, P., and Diamond, G. (1997) Isolation and characterization of pleurocidin, an antimicrobial peptide in the skin secretions of winter flounder, *J. Biol. Chem. 272*, 12008.
8. Park, C. J., Park, C. B., Hong, S. S., Lee, H. S., Lee, S. Y., and Kim, S. C. (2000) Characterization and cDNA cloning of two glycine- and histidine-rich antimicrobial peptides from the roots of shepherd's purse, *Capsella bursa-pastoris*, *Plant Mol. Biol. 44*, 187.
9. Hancock, R. E. (1997) Peptide antibiotics, *Lancet 349*, 418.
10. Zhang, L. J., Rozek, A., and Hancock, R. E. W. (2001) Interaction of cationic antimicrobial peptides with model membranes, *J. Biol. Chem. 276*, 35714.
11. Wade, D., Boman, A., Wahlin, B., Drain, C. M., Andreu, D., Boman, H. G., and (1990) Merrifield, R. B. All-D amino acid-containing channel-forming antibiotic peptides, *Proc. Natl. Acad. Sci. U.S.A 87*, 4761.
12. Bessalle, R., Kapitkovsky, A., Gorea, A., Shalit, I., and Fridkin, M. (1990) All-D-magainin: chirality, antimicrobial activity and proteolytic resistance, *FEBS Lett. 274*, 151.
13. Yasin, B., Lehrer, R. I., Harwig, S. S., and Wagar, E. A. (1996) Protegrins: structural requirements for inactivating elementary bodies of *Chlamydia trachomatis*, *Infect. Immun. 64*, 4863.
14. Epand, R. M., and Vogel, H. J. (1999) Diversity of antimicrobial peptides and their mechanisms of action, *Biochim. Biophys. Acta 1462*, 11.
15. Dathe, M., and Wieprecht, T. (1999) Structural features of helical antimicrobial peptides: their potential to modulate activity on model membranes and biological cells, *Biochim. Biophys. Acta 1462*, 71.
16. Cafiso, D. S. (1994) Alamethicin: a peptide model for voltage gating and protein-membrane interactions, *Annu. Rev. Biophys. Biomol. Struct. 23*, 141.
17. Wu, M., Maier, E., Benz, R., and Hancock, R. E. (1999) Mechanism of interaction of different classes of cationic antimicrobial peptides with planar bilayers and with the cytoplasmic membrane of *Escherichia coli*, *Biochemistry 38*, 7235.
18. Friedrich, C. L., Moyles, D., Beveridge, T. J., and Hancock, R. E. (2000) Antibacterial action of structurally diverse cationic peptides on gram-positive bacteria, *Antimicrob. Agents Chemother. 44*, 2086.
19. Lehrer, R. I., Barton, A., Daher, K. A., Harwig, S. S., Ganz, T., and (1989) Selsted, M. E. Interaction of human defensins with *Escherichia coli*. Mechanism of bactericidal activity, *J. Clin. Invest. 84*, 553.
20. Bechinger, B., Zasloff, M., and Opella, S. J. (1998) Structure and dynamics of the antibiotic peptide PGLa in membranes by solution and solid-state nuclear magnetic resonance spectroscopy, *Biophys. J. 74*, 981.
21. Bechinger, B., Zasloff, M., and Opella, S. J. (1992) Structure and interactions of magainin antibiotic peptides in lipid bilayers: a solid-state nuclear magnetic resonance investigation, *Biophys. J. 62*, 12.
22. Bechinger, B., Zasloff, M., and Opella, S. J. (1993) Structure and orientation of the antibiotic peptide magainin in membranes by solid-state nuclear magnetic resonance spectroscopy, *Protein Sci. 2*, 2077.
23. Matsuzaki, K., Murase, O., Tokuda, H., Funakoshi, S., Fujii, N., and Miyajima, K. (1994) Orientational and aggregational states of magainin 2 in phospholipid bilayers, *Biochemistry 33*, 3342.
24. Matsuzaki, K., Harada, M., Handa, T., Funakoshi, S., Fujii, N., Yajima, H., and Miyajima, K. (1989) Magainin 1-induced leakage of entrapped calcein out of negatively-charged lipid vesicles, *Biochim. Biophys. Acta 981*, 130.
25. Baumann, G., and Mueller, P. (1974) A molecular model of membrane excitability, *J. Supramol. Struct. 2*, 538.
26. Ludtke, S. J., He, K., Heller, W. T., Harroun, T. A., Yang, L., and Huang, H. W. (1996) Membrane pores induced by magainin, *Biochemistry 35*, 13723.
27. Matsuzaki, K., Murase, O., Fujii, N., and Miyajima, K. (1996) An antimicrobial peptide, magainin 2, induced rapid flip-flop of phospholipids coupled with pore formation and peptide translocation, *Biochemistry 35*, 11361.
28. Pouny, Y., and Shai, Y. (1992) Interaction of D-amino acid incorporated analogues of pardaxin with membranes, *Biochemistry 31*, 9482.
29. Gazit, E., Boman, A., Boman, H. G., and Shai, Y. (1995) Interaction of the mammalian antibacterial peptide cecropin P1 with phospholipid vesicles, *Biochemistry 34*, 11479.
30. Pouny, Y., Rapaport, D., Mor, A., Nicolas, P., and Shai, Y. (1992) Interaction of antimicrobial dermaseptin and its fluorescently labeled analogues with phospholipid membranes, *Biochemistry 31*, 12416.
31. Yoshida, K., Mukai, Y., Niidome, T., Takashi, C., Tokunaga, Y., Hatakeyama, T., and Aoyagi, H. (2001) Interaction of pleurocidin and its analogs with phospholipid membrane and their antibacterial activity, *J. Pept. Res. 57*, 119.
32. Saint, N., Cadiou, H., Bessin, Y., Molle, G. (2002) Antibacterial peptide pleurocidin forms ion channels in planar lipid bilayers, *Biochim. Biophys. Acta 1564*, 359.
33. Lauterwein, J., Bosch, C., Brown, L. R., and Wuthrich, K. (1979) Physicochemical studies of the protein-lipid interactions in melittin-containing micelles, *Biochim. Biophys. Acta 556*, 244.
34. Gottlieb, H. E., Kotlyar, V., and Nudelman, A. (1997) NMR chemical shifts of common laboratory solvents as trace impurities, *J. Org. Chem. 62*, 7512.
35. Wishart, D. S., Bigam, C. G., Yao, J., Abildgaard, F., Dyson, H. J., Oldfield, E., Markley, J. L., and Sykes, B. D. (1995) 1H, 13C and 15N chemical shift referencing in biomolecular NMR, *J. Biomol. NMR 6*, 135.
36. Barker, P. B., Golay, X., Artemov, D., Ouwerkerk, R., Smith, M. A., and Shaka, A. J. (2001) Broadband proton decoupling for in vivo brain spectroscopy in humans, *Magn. Reson. Med. 45*, 226.
37. Piotto, M., Saudek, V., Sklenar, V. (1992) Gradient-tailored excitation for single-quantum NMR-spectroscopy of aqueous-solutions, *J. Biomol. NMR 2*, 661.
38. Sklenar, V., Piotto, M., Leppik, R., and Saudek, V. (1993) Gradient-tailored water suppression for H-1-N-15 HSQC experiments optimized to retain full sensitivity, *J. Magn. Reson. Ser. A 102*, 241.
39. Andersson, P., Weigelt, J., and Otting, G. (1998) Spin-state selection filters for the measurement of heteronuclear one-bond coupling constants, *J. Biomol. NMR 12*, 435.
40. Marion, D., Ikura, M., and Bax, A. (1989) Improved solvent suppression in one-dimensional and two-dimensional NMR-spectra by convolution of time-domain data, *J. Magn. Reson. 84*, 425.
41. Jeener, J., Meier, B. H., Bachmann, P., and Ernst, R. R. (1979) Investigation of exchange processes by two-dimensional NMR spectroscopy, *J. Chem. Phys. 71*, 4546.
42. Griesinger, C., Otting, G., Wuthrich, K., Ernst, R. R. (1988) Clean TOCSY for H-1 Spin System-Identification in Macromolecules, *J. Am. Chem. Soc. 110*, 7870.
43. Bax, A., and Davis, D. G. (1985) MLEV-17-based two-dimensional homonuclear magnetization transfer spectroscopy, *J. Magn. Reson. 65*, 355.
44. Talluri, S., and Wagner, G. (1996) An optimized 3D NOESY-HSQC, *J. Magn. Reson. Ser. B 112*, 200.
45. Vuister, G. W., and Bax, A. (1992) Resolution enhancement and spectral editing of uniformly C-13-enriched proteins by homonuclear broad-band C-13 decoupling, *J. Magn. Reson. 98*, 428.
46. Schleucher, J., Schwendinger, M., Sattler, M., Schmidt, P., Schedletzky, O., Glaser, S. J., Sorensen, O. W., Griesinger, C. (1994) A general enhancement scheme in heteronuclear multidimensional NMR employing pulsed field gradients, *J. Biomol. NMR 4*, 301.
47. Barkhuijsen, H., de Beer, R., Bovee, W. M., Creyghton, J. H., and van Ormondt, D. (1985) Application of linear prediction and singular value decomposition (LPSVD) to determine NMR frequencies and intensities from the FID, *Magn. Reson. Med. 2*, 86.
48. Farrow, N. A., Zhang, O., Forman-Kay, J. D., and Kay, L. E. (1994) A heteronuclear correlation experiment for simultaneous determination of 15N longitudinal decay and chemical exchange rates of systems in slow equilibrium, *J. Biomol. NMR 4*, 727.

49. Farrow, N. A., Muhandiram, R., Singer, A. U., Pascal, S. M., Kay, C. M., Gish, G., Shoelson, S. E., Pawson, T., Forman-Kay, J. D., and Kay, L. E. (1994) Backbone dynamics of a free and phosphopeptide-complexed Src homology 2 domain studied by 15N NMR relaxation, *Biochemistry 33*, 5984.
50. Wu, D. H., Chen, A. D., and Johnson, C. S. (1995) An improved diffusion-ordered spectroscopy experiment incorporating bipolar-gradient pulses, *J. Magn. Reson. Ser. A 115*, 260.
51. Johnson, C. S. (1999) Diffusion ordered nuclear magnetic resonance spectroscopy: principles and applications, *Prog. Nucl. Magn. Reson. Spectrosc. 34*, 203.
52. Goddard, T. D., and Kneller, D. G. (2002) *Sparky 3*, University of California, San Francisco.
53. Wuthrich, K. (1986) *NMR of proteins and nucleic acids*, John Wiley and Sons, New York.
54. Opella, S. J., Marassi, F. M., Gesell, J. J., Valente, A. P., Kim, Y., Oblatt-Montal, M., and Montal, M. (1999) Structures of the M2 channel-lining segments from nicotinic acetylcholine and NMDA receptors by NMR spectroscopy, *Nat. Struct. Biol. 6*, 374.
55. Wishart, D. S., Sykes, B. D., and Richards, F. M. (1992) The chemical-shift index—A fast and simple method for the assignment of protein secondary structure through NMR-spectroscopy, *Biochemistry 31*, 1647.
56. Wishart, D. S., and Sykes, B. D. (1994) Chemical-shifts as a tool for structure determination, *Methods Enzymol.*, 363−392.
57. Baker, E. N., and Hubbard, R. E. (1984) Hydrogen bonding in globular proteins, *Prog. Biophys. Mol. Biol. 44*, 97.
58. Mitchell, J. B. O., and Price, S. L. (1990) The nature of the N−H O═C hydrogen-bond—An intermolecular perturbation-theory study of the formamide formaldehyde complex, *J. Comput. Chem. 11*, 1217.
59. Corcoran, J. A., Syvitski, R., Top, D., Epand, R. M., Epand, R. F., Jakeman, D., and Duncan, R. (2004) Myristoylation, a protruding loop, and structural plasticity are essential features of a nonenveloped virus fusion peptide motif, *J. Biol. Chem. 279*, 51386.
60. Kuszewski, J., Nilges, M., and Brunger, A. T. (1992) Sampling and efficiency of metric matrix distance geometry—A novel partial metrization algorithm, *J. Biomol. NMR 2*, 33.
61. Nilges, M., Clore, G. M., and Gronenborn, A. M. (1988) Determination of three-dimensional structures of proteins from interproton distance data by hybrid distance geometry-dynamical simulated annealing calculations, *FEBS Lett. 229*, 317.
62. Nilges, M., Kuszewski, J., and Brunger, A. T. (1991) *Computational aspects of the study of biological macromolecules by NMR*, Plenum Press, New York.
63. Laskowski, R. A., MacArthur, M. W., Moss, D. S., and Thornton, J. M. (1993) PROCHECK: a program to check the stereochemical quality of protein structures, *J. Appl. Crystallogr. 26*, 283.
64. Laskowski, R. A., Rullmann, J. A. C., MacArthur, M. W., Kaptein, R., and Thornton, J. M. (1996) AQUA and PROCHECK-NMR: Programs for checking the quality of protein structures solved by NMR, *J. Biomol. NMR 8*, 477.
65. Morris, A. L., MacArthur, M. W., Hutchinson, E. G., and Thornton, J. M. (1992) Stereochemical quality of protein structure coordinates, *Proteins 12*, 345.
66. Fasman, G. D. (1983) *Handbook of biochemistry and molecular biology*, CRC, Boca Raton, FL.
67. Harpaz, Y., Gerstein, M., and Chothia, C. (1994) Volume changes on protein-folding, *Structure 2*, 641.
68. Vinogradova, O., Sonnichsen, F., and Sanders, C. R. (1998) On choosing a detergent for solution NMR studies of membrane proteins, *J. Biomol. NMR 11*, 381.
69. Lipari, G., and Szabo, A. (1982) Analysis of NMR relaxation data on macromolecules using the model-free approach, *Biophys. J. 37*, A380.
70. Lipari, G., and Szabo, A. (1982) Model-free approach to the interpretation of nuclear magnetic-resonance relaxation in macromolecules. 2. Analysis of experimental results, *J. Am. Chem. Soc. 104*, 4559.
71. Lipari, G., and Szabo, A. (1982) Model-Free approach to the interpretation of nuclear magnetic-resonance relaxation in macromolecules. 1. Theory and range of validity, *J. Am. Chem. Soc. 104*, 4546.
72. Lipari, G., Szabo, A., and Levy, R. M. (1982) Protein dynamics and NMR relaxation—Comparison of simulations with experiment, *Nature 300*, 197.
73. Palmer, A. G., III, Rance, M., and Wright, P. E. (1991) Intramolecular motions of a zinc finger DNA-binding domain from Xfin characterized by proton-detected natural abundance carbon-13 heteronuclear NMR spectroscopy, *J. Am. Chem. Soc. 113*, 4371.
74. Mandel, A. M., Akke, M., and Palmer, A. G., III (1995) Backbone dynamics of *Escherichia coli* ribonuclease HI: correlations with structure and function in an active enzyme, *J. Mol. Biol. 246*, 144.
75. Sanders, C. R., and Oxenoid, K. (2000) Customizing model membranes and samples for NMR spectroscopic studies of complex membrane proteins, *Biochim. Biophys. Acta 1508*, 129.
76. Almeida, F. C. L., and Opella, S. J. (1997) fd coat protein structure in membrane environments: Structural dynamics of the loop between the hydrophobic trans-membrane helix and the amphipathic in-plane helix, *J. Mol. Biol. 270*, 481.
77. Papavoine, C. H., Remerowski, M. L., Horstink, L. M., Konings, R. N., Hilbers, C. W., and van de Ven, F. J. (1997) Backbone dynamics of the major coat protein of bacteriophage M13 in detergent micelles by 15N nuclear magnetic resonance relaxation measurements using the model-free approach and reduced spectral density mapping, *Biochemistry 36*, 4015.
78. Fernandez, C., Hilty, C., Wider, G., and Wuthrich, K. (2002) Lipid-protein interactions in DHPC micelles containing the integral membrane protein OmpX investigated by NMR spectroscopy, *Proc. Natl. Acad. Sci. U.S.A. 99*, 13533.
79. Hu, W., and Cross, T. A. (1995) Tryptophan hydrogen bonding and electric dipole moments: functional roles in the gramicidin channel and implications for membrane proteins, *Biochemistry 34*, 14147.
80. Schiffer, M., Chang, C. H., and Stevens, F. J. (1992) The functions of tryptophan residues in membrane proteins, *Protein Eng. 5*, 213.
81. Otting, G., Liepinsh, E., and Wuthrich, K. (1991) Protein hydration in aqueous-solution, *Science 254*, 974.

BI0504005